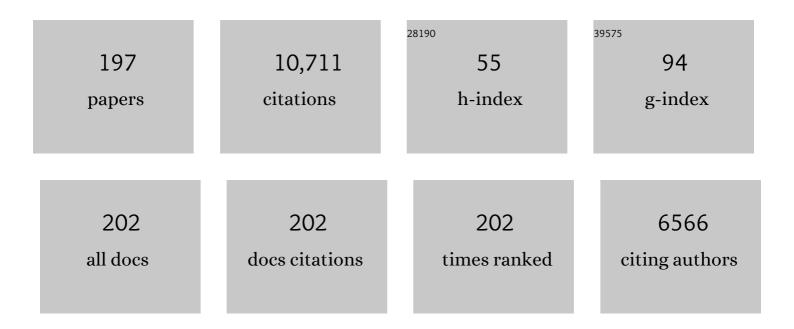
## Ravinder Reddy

List of Publications by Year in descending order

Source: https://exaly.com/author-pdf/9374224/publications.pdf Version: 2024-02-01



#	Article	IF	CITATIONS
1	Glutamateâ€weighted CEST (gluCEST) imaging for mapping neurometabolism: An update on the state of the art and emerging findings from <i>in vivo</i> applications. NMR in Biomedicine, 2023, 36, .	1.6	9
2	miRNAs as novel immunoregulators in cancer. Seminars in Cell and Developmental Biology, 2022, 124, 3-14.	2.3	11
3	In vivo assessment of OXPHOS capacity using 3ÂT CrCEST MRI in Friedreich's ataxia. Journal of Neurology, 2022, 269, 2527-2538.	1.8	2
4	Integrating 1H MRS and deuterium labeled glucose for mapping the dynamics of neural metabolism in humans. NeuroImage, 2022, 251, 118977.	2.1	14
5	Genetics of glutamate and its receptors in autism spectrum disorder. Molecular Psychiatry, 2022, 27, 2380-2392.	4.1	39
6	Coherence pathway analysis of J-coupled lipids and lactate and effective suppression of lipids upon the selective multiple quantum coherence lactate editing sequence. Biomedical Physics and Engineering Express, 2022, 8, 035004.	0.6	1
7	Glutamate-Weighted Magnetic Resonance Imaging (GluCEST) Detects Effects of Transcranial Magnetic Stimulation to the Motor Cortex. NeuroImage, 2022, 256, 119191.	2.1	10
8	Review and consensus recommendations on clinical <scp>APT</scp> â€weighted imaging approaches at <scp>3T</scp> : Application to brain tumors. Magnetic Resonance in Medicine, 2022, 88, 546-574.	1.9	79
9	Characterizing the neurological phenotype of the hyperinsulinism hyperammonemia syndrome. Orphanet Journal of Rare Diseases, 2022, 17, .	1.2	5
10	Recovery kinetics of creatine in mild plantar flexion exercise using 3D creatine CEST imaging at 7 Tesla. Magnetic Resonance in Medicine, 2021, 85, 802-817.	1.9	15
11	Fast automatic segmentation of thalamic nuclei from MP2RAGE acquisition at 7 Tesla. Magnetic Resonance in Medicine, 2021, 85, 2781-2790.	1.9	11
12	Quantitative imaging of the spine in adolescent idiopathic scoliosis: shifting the paradigm from diagnostic to comprehensive prognostic evaluation. European Journal of Orthopaedic Surgery and Traumatology, 2021, 31, 1273-1285.	0.6	2
13	Diminished reward responsiveness is associated with lower reward network GluCEST: an ultra-high field glutamate imaging study. Molecular Psychiatry, 2021, 26, 2137-2147.	4.1	10
14	Cytokine-chemokine network driven metastasis in esophageal cancer; promising avenue for targeted therapy. Molecular Cancer, 2021, 20, 2.	7.9	76
15	Insights Into the Role of CircRNAs: Biogenesis, Characterization, Functional, and Clinical Impact in Human Malignancies. Frontiers in Cell and Developmental Biology, 2021, 9, 617281.	1.8	53
16	Effect of offsetâ€frequency step size and interpolation methods on chemical exchange saturation transfer MRI computation in human brain. NMR in Biomedicine, 2021, 34, e4468.	1.6	4
17	Improved method for postâ€processing correction of <i>B</i> <sub>1</sub> inhomogeneity in glutamateâ€weighted CEST images of the human brain. NMR in Biomedicine, 2021, 34, e4503.	1.6	11
18	Multimodality assessment of heart failure with preserved ejection fraction skeletal muscle reveals differences in the machinery of energy fuel metabolism. ESC Heart Failure, 2021, 8, 2698-2712.	1.4	16

#	Article	IF	CITATIONS
19	7T Magnetic Resonance Imaging Quantification of Brain Glutamate in Acute Ischaemic Stroke. Journal of Stroke, 2021, 23, 281-284.	1.4	5
20	Genetic variations influence brain changes in patients with attention-deficit hyperactivity disorder. Translational Psychiatry, 2021, 11, 349.	2.4	37
21	Role of NAD+ in regulating cellular and metabolic signaling pathways. Molecular Metabolism, 2021, 49, 101195.	3.0	104
22	Volumetric glutamate imaging (GluCEST) using 7T MRI can lateralize nonlesional temporal lobe epilepsy: A preliminary study. Brain and Behavior, 2021, 11, e02134.	1.0	7
23	MXene-infused bioelectronic interfaces for multiscale electrophysiology and stimulation. Science Translational Medicine, 2021, 13, eabf8629.	5.8	68
24	Ubiquitin-specific peptidase 37: an important cog in the oncogenic machinery of cancerous cells. Journal of Experimental and Clinical Cancer Research, 2021, 40, 356.	3.5	8
25	Singleâ€Voxel <sup>1</sup> H MR spectroscopy of cerebral nicotinamide adenine dinucleotide (NAD <sup>+</sup> ) in humans at 7T using a 32â€channel volume coil. Magnetic Resonance in Medicine, 2020, 83, 806-814.	1.9	26
26	Glutamate-Weighted CEST Contrast After Removal of Magnetization Transfer Effect in Human Brain and Rat Brain with Tumor. Molecular Imaging and Biology, 2020, 22, 1087-1101.	1.3	11
27	Single-Cell Analyses Identify Brain Mural Cells Expressing CD19 as Potential Off-Tumor Targets for CAR-T Immunotherapies. Cell, 2020, 183, 126-142.e17.	13.5	269
28	A quantitative meta-analysis of brain glutamate metabolites in aging. Neurobiology of Aging, 2020, 95, 240-249.	1.5	33
29	Genetics of structural and functional brain changes in autism spectrum disorder. Translational Psychiatry, 2020, 10, 229.	2.4	63
30	Non-invasive biomarkers for monitoring the immunotherapeutic response to cancer. Journal of Translational Medicine, 2020, 18, 471.	1.8	15
31	The Myelin Water Fraction Serves as a Marker for Age-Related Myelin Alterations in the Cerebral White Matter – A Multiparametric MRI Aging Study. Frontiers in Neuroscience, 2020, 14, 136.	1.4	38
32	Genetic and Neuroimaging Approaches to Understanding Post-Traumatic Stress Disorder. International Journal of Molecular Sciences, 2020, 21, 4503.	1.8	21
33	Claudin-1, A Double-Edged Sword in Cancer. International Journal of Molecular Sciences, 2020, 21, 569.	1.8	76
34	1H magnetic resonance spectroscopy of 2H-to-1H exchange quantifies the dynamics of cellular metabolism in vivo. Nature Biomedical Engineering, 2020, 4, 335-342.	11.6	40
35	Zone- and layer-specific differences in proteoglycan content in patellofemoral pain syndrome are detectable on T11-MRI. Skeletal Radiology, 2020, 49, 1397-1402.	1.2	1
36	Accelerating GluCEST imaging using deep learning for B <sub>0</sub> correction. Magnetic Resonance in Medicine, 2020, 84, 1724-1733.	1.9	21

#	Article	IF	CITATIONS
37	Functional In Vivo Imaging of Tumors. Cancer Treatment and Research, 2020, 180, 3-50.	0.2	1
38	MON-110 Utilization of GluCEST, a Novel Neuroimaging Technique, to Characterize the Brain Phenotype in Hyperinsulinism/Hyperammonemia Syndrome. Journal of the Endocrine Society, 2020, 4, .	0.1	1
39	Sugar alcohol provides imaging contrast in cancer detection. Scientific Reports, 2019, 9, 11092.	1.6	7
40	Evaluating the feasibility of creatineâ€weighted CEST MRI in human brain at 7 T using a Zâ€spectral fitting approach. NMR in Biomedicine, 2019, 32, e4176.	1.6	24
41	Glutamate weighted imaging contrast in gliomas with 7†Tesla magnetic resonance imaging. NeuroImage: Clinical, 2019, 22, 101694.	1.4	50
42	Association of genes with phenotype in autism spectrum disorder. Aging, 2019, 11, 10742-10770.	1.4	23
43	In vivo GluCEST MRI: Reproducibility, background contribution and source of glutamate changes in the MPTP model of Parkinson's disease. Scientific Reports, 2018, 8, 2883.	1.6	38
44	Age-Related Measurements of the Myelin Water Fraction derived from 3D multi-echo GRASE reflect Myelin Content of the Cerebral White Matter. Scientific Reports, 2018, 8, 14991.	1.6	38
45	Reproducibility of 2 <scp>D</scp> <scp>G</scp> lu <scp>CEST</scp> in healthy human volunteers at 7 <scp>T</scp> . Magnetic Resonance in Medicine, 2018, 80, 2033-2039.	1.9	32
46	Glutamate-Weighted Chemical Exchange Saturation Transfer Magnetic Resonance Imaging Detects Glutaminase Inhibition in a Mouse Model of Triple-Negative Breast Cancer. Cancer Research, 2018, 78, 5521-5526.	0.4	19
47	High quality threeâ€dimensional gagCEST imaging of in vivo human knee cartilage at 7 Tesla. Magnetic Resonance in Medicine, 2017, 77, 1866-1873.	1.9	44
48	Perfusion has no effect on the <i>in vivo</i> CEST effect from Cr (CrCEST) in skeletal muscle. NMR in Biomedicine, 2017, 30, e3673.	1.6	12
49	Longitudinal imaging reveals subhippocampal dynamics in glutamate levels associated with histopathologic events in a mouse model of tauopathy and healthy mice. Hippocampus, 2017, 27, 285-302.	0.9	47
50	Non-caloric sweetener provides magnetic resonance imaging contrast for cancer detection. Journal of Translational Medicine, 2017, 15, 119.	1.8	13
51	Molecular imaging biomarkers for cell-based immunotherapies. Journal of Translational Medicine, 2017, 15, 140.	1.8	11
52	Creatine CEST MRI for Differentiating Gliomas with Different Degrees of Aggressiveness. Molecular Imaging and Biology, 2017, 19, 225-232.	1.3	45
53	Lisdexamfetamine Effects on Executive Activation and Neurochemistry in Menopausal Women with Executive Function Difficulties. Neuropsychopharmacology, 2017, 42, 437-445.	2.8	23

54 Chapter 18 Creatine Chemical Exchange Saturation Transfer Imaging. , 2017, , 427-446.

0

#	Article	IF	CITATIONS
55	Fully automated macromolecule suppressed single voxel glutamate spectroscopy (FAMOUS SVGS). Journal of Translational Medicine, 2016, 14, 220.	1.8	1
56	Mapping the alterations in glutamate with Glu <scp>CEST MRI</scp> in a mouse model of dopamine deficiency. Journal of Neurochemistry, 2016, 139, 432-439.	2.1	43
57	TlϕMagnetic Resonance Imaging to Assess Cartilage Damage After Primary Shoulder Dislocation. American Journal of Sports Medicine, 2016, 44, 2800-2806.	1.9	13
58	Lactate Chemical Exchange Saturation Transfer (LATEST) Imaging in vivo: A Biomarker for LDH Activity. Scientific Reports, 2016, 6, 19517.	1.6	62
59	Localized, gradientâ€reversed ultrafast zâ€spectroscopy in vivo at 7T. Magnetic Resonance in Medicine, 2016, 76, 1039-1046.	1.9	7
60	Characterization of viscosupplementation formulations using chemical exchange saturation transfer (ViscoCEST). Journal of Translational Medicine, 2016, 14, 92.	1.8	10
61	Muscle oxidative phosphorylation quantitation using creatine chemical exchange saturation transfer (CrCEST) MRI in mitochondrial disorders. JCI Insight, 2016, 1, e88207.	2.3	38
62	CEST signal at 2 ppm (CEST@2ppm) from <i>Z</i> â€spectral fitting correlates with creatine distribution in brain tumor. NMR in Biomedicine, 2015, 28, 1-8.	1.6	180
63	T1Ï•MRI of healthy and fibrotic human livers at 1.5ÂT. Journal of Translational Medicine, 2015, 13, 292.	1.8	42
64	Molecular magnetic resonance imaging in cancer. Journal of Translational Medicine, 2015, 13, 313.	1.8	79
65	Imaging technologies from bench to bedside. Journal of Translational Medicine, 2015, 13, 97.	1.8	5
66	Visualization of Injectable Hydrogels Using Chemical Exchange Saturation Transfer MRI. ACS Biomaterials Science and Engineering, 2015, 1, 227-237.	2.6	19
67	Glutamate imaging (GluCEST) lateralizes epileptic foci in nonlesional temporal lobe epilepsy. Science Translational Medicine, 2015, 7, 309ra161.	5.8	156
68	T1rho Magnetic Resonance Imaging at 3T Detects Knee Cartilage Changes After Viscosupplementation. Orthopedics, 2015, 38, e604-10.	0.5	6
69	High Resolution T1ϕMapping of In Vivo Human Knee Cartilage at 7T. PLoS ONE, 2014, 9, e97486.	1.1	42
70	High Resolution Mapping of Modafinil Induced Changes in Glutamate Level in Rat Brain. PLoS ONE, 2014, 9, e103154.	1.1	17
71	In vivo chemical exchange saturation transfer imaging of creatine (CrCEST) in skeletal muscle at 3T. Journal of Magnetic Resonance Imaging, 2014, 40, 596-602.	1.9	77
72	Glutaminase catalyzes reaction of Glutamate to GABA. Biochemical and Biophysical Research Communications, 2014, 448, 361-364.	1.0	7

#	Article	IF	CITATIONS
73	A technique for in vivo mapping of myocardial creatine kinase metabolism. Nature Medicine, 2014, 20, 209-214.	15.2	168
74	In vivo measurement of glutamate loss is associated with synapse loss in a mouse model of tauopathy. NeuroImage, 2014, 101, 185-192.	2.1	57
75	Breast Cancer Redox Heterogeneity Detectable with Chemical Exchange Saturation Transfer (CEST) MRI. Molecular Imaging and Biology, 2014, 16, 670-679.	1.3	27
76	Method for highâ€resolution imaging of creatine in vivo using chemical exchange saturation transfer. Magnetic Resonance in Medicine, 2014, 71, 164-172.	1.9	138
77	In vivo Magnetic Resonance Imaging of Tumor Protease Activity. Scientific Reports, 2014, 4, 6081.	1.6	57
78	Imaging Modalities for Studying Disc Pathology. , 2014, , 201-212.		0
79	On <i>B</i> <sub>1</sub> inhomogeneity correction of in vivo human brain glutamate chemical exchange saturation transfer contrast at 7T. Magnetic Resonance in Medicine, 2013, 69, 818-824.	1.9	79
80	Chemical Exchange Saturation Transfer (CEST) Imaging: Description of Technique and Potential Clinical Applications. Current Radiology Reports, 2013, 1, 102-114.	0.4	140
81	Imaging of glutamate neurotransmitter alterations in Alzheimer's disease. NMR in Biomedicine, 2013, 26, 386-391.	1.6	116
82	Imaging of glutamate in the spinal cord using GluCEST. NeuroImage, 2013, 77, 262-267.	2.1	62
83	MICEST: A potential tool for non-invasive detection of molecular changes in Alzheimer's disease. Journal of Neuroscience Methods, 2013, 212, 87-93.	1.3	57
84	Mapping glutamate in subcortical brain structures using highâ€resolution GluCEST MRI. NMR in Biomedicine, 2013, 26, 1278-1284.	1.6	73
85	Skeletal Muscle MR Imaging Beyond Protons: With a Focus on Sodium MRI in Musculoskeletal Applications. Medical Radiology, 2013, , 115-133.	0.0	1
86	Blood Oxygen Level Dependent Magnetization Transfer (BOLDMT) Effect. Advances in Experimental Medicine and Biology, 2013, 765, 31-37.	0.8	2
87	Characterizing Prostate Tumor Mouse Xenografts with CEST and MT-MRI and Redox Scanning. Advances in Experimental Medicine and Biology, 2013, 765, 39-45.	0.8	12
88	Magnetic resonance imaging of glutamate. Nature Medicine, 2012, 18, 302-306.	15.2	544
89	The Impact of Gabapentin Administration on Brain GABA and Glutamate Concentrations: A 7T 1H-MRS Study. Neuropsychopharmacology, 2012, 37, 2764-2771.	2.8	113
90	Quantitative cartilage degeneration associated with spontaneous osteoarthritis in a guinea pig model. Journal of Magnetic Resonance Imaging, 2012, 35, 891-898.	1.9	20

#	Article	IF	CITATIONS
91	Absolute cerebral blood flow quantification with pulsed arterial spin labeling during hyperoxia corrected with the simultaneous measurement of the longitudinal relaxation time of arterial blood. Magnetic Resonance in Medicine, 2012, 67, 1556-1565.	1.9	27
92	Investigation of chemical exchange at intermediate exchange rates using a combination of chemical exchange saturation transfer (CEST) and spinâ€locking methods (CESTrho). Magnetic Resonance in Medicine, 2012, 68, 107-119.	1.9	22
93	Chemical exchange saturation transfer magnetic resonance imaging of human knee cartilage at 3 T and 7 T. Magnetic Resonance in Medicine, 2012, 68, 588-594.	1.9	137
94	Exchange rates of creatine kinase metabolites: feasibility of imaging creatine by chemical exchange saturation transfer MRI. NMR in Biomedicine, 2012, 25, 1305-1309.	1.6	157
95	Blood oxygen level dependent angiography (BOLDangio) and its potential applications in cancer research. NMR in Biomedicine, 2012, 25, 1125-1132.	1.6	10
96	In vivo mapping of brain myo-inositol. NeuroImage, 2011, 54, 2079-2085.	2.1	216
97	Characterization of paramagnetic effects of molecular oxygen on blood oxygenation levelâ€dependentâ€modulated hyperoxic contrast studies of the human brain. Magnetic Resonance in Medicine, 2011, 66, 794-801.	1.9	21
98	Knee Articular Cartilage Damage in Osteoarthritis: Analysis of MR Image Biomarker Reproducibility in ACRIN-PA 4001 Multicenter Trial. Radiology, 2011, 258, 832-842.	3.6	135
99	The Fate of Oral Glucosamine Traced by <sup>13</sup> C Labeling in the Dog. Cartilage, 2011, 2, 279-285.	1.4	4
100	NMR Metabolic and Physiological Markers of Therapeutic Response. Advances in Experimental Medicine and Biology, 2011, 701, 129-135.	0.8	4
101	Characterizing Breast Cancer Mouse Xenografts with T1Ï•-MRI. Advances in Experimental Medicine and Biology, 2011, 701, 137-142.	0.8	3
102	Frontiers in Molecular Imaging of Cartilage: Future Developments. , 2011, , 213-227.		2
103	Validation of Sodium Magnetic Resonance Imaging of Intervertebral Disc. Spine, 2010, 35, 505-510.	1.0	55
104	<i>T</i> <sub>1</sub> ï•MRI quantification of arthroscopically confirmed cartilage degeneration. Magnetic Resonance in Medicine, 2010, 63, 1376-1382.	1.9	49
105	Magnetization transfer ratio mapping of intervertebral disc degeneration. Magnetic Resonance in Medicine, 2010, 64, 1520-1528.	1.9	21
106	Rotating frame spin lattice relaxation in a swine model of chronic, left ventricular myocardial infarction. Magnetic Resonance in Medicine, 2010, 64, 1453-1460.	1.9	43
107	Measurement of intervertebral disc pressure with <i>T</i> <sub>1ï</sub> MRI. Magnetic Resonance in Medicine, 2010, 64, 1721-1727.	1.9	14
108	Imaging Cartilage Physiology. Topics in Magnetic Resonance Imaging, 2010, 21, 291-296.	0.7	20

#	Article	IF	CITATIONS
109	Mapping of cerebral oxidative metabolism with MRI. Proceedings of the National Academy of Sciences of the United States of America, 2010, 107, 11787-11792.	3.3	23
110	Quantitative magnetic resonance and optical imaging biomarkers of melanoma metastatic potential. Proceedings of the National Academy of Sciences of the United States of America, 2009, 106, 6608-6613.	3.3	86
111	Spinâ€locked balanced steadyâ€state freeâ€precession (slSSFP). Magnetic Resonance in Medicine, 2009, 62, 993-1001.	1.9	6
112	Detection of lactate with a hadamard slice selected, selective multiple quantum coherence, chemical shift imaging sequence (HDMDâ€SelMQCâ€CSI) on a clinical MRI scanner: Application to tumors and muscle ischemia. Magnetic Resonance in Medicine, 2009, 62, 1404-1413.	1.9	29
113	Estimation of the regional cerebral metabolic rate of oxygen consumption with proton detected 170 MRI during precision 1702 inhalation in swine. Journal of Neuroscience Methods, 2009, 179, 29-39.	1.3	29
114	Single Shot T1ϕMagnetic Resonance Imaging Of Metabolically Generated Water In Vivo. Advances in Experimental Medicine and Biology, 2009, 645, 279-286.	0.8	8
115	T1Ïâ€prepared balanced gradient echo for rapid 3D T1Ï•MRI. Journal of Magnetic Resonance Imaging, 2008, 28, 744-754.	1.9	67
116	Compensation for spin-lock artifacts using an off-resonance rotary echo inT1ïoff-weighted imaging. Magnetic Resonance in Medicine, 2007, 57, 2-7.	1.9	26
117	Frontiers in musculoskeletal MRI: Articular cartilage. Journal of Magnetic Resonance Imaging, 2007, 25, 339-344.	1.9	27
118	Advances in Magnetic Resonance Imaging for the Assessment of Degenerative Disc Disease of the Lumbar Spine. Seminars in Spine Surgery, 2007, 19, 65-71.	0.1	29
119	Artifacts in T1ï•weighted imaging: Compensation for B1 and B0 field imperfections. Journal of Magnetic Resonance, 2007, 186, 75-85.	1.2	142
120	Magic sandwich echo relaxation mapping of anisotropic systems. Magnetic Resonance Imaging, 2007, 25, 433-438.	1.0	6
121	Assessment of Human Disc Degeneration and Proteoglycan Content Using T1ϕweighted Magnetic Resonance Imaging. Spine, 2006, 31, 1253-1257.	1.0	187
122	In vivo quantification of human lumbar disc degeneration using T1ϕweighted magnetic resonance imaging. European Spine Journal, 2006, 15, 338-344.	1.0	106
123	Sodium andT1ϕMRI for molecular and diagnostic imaging of articular cartilage. NMR in Biomedicine, 2006, 19, 781-821.	1.6	259
124	T1ϕrelaxation mapping in human osteoarthritis (OA) cartilage: Comparison of T1ϕwith T2. Journal of Magnetic Resonance Imaging, 2006, 23, 547-553.	1.9	296
125	A pulse sequence for rapid in vivo spin-locked MRI. Journal of Magnetic Resonance Imaging, 2006, 23, 591-596.	1.9	29
126	In vivo measurement of plaque burden in a mouse model of Alzheimer's disease. Journal of Magnetic Resonance Imaging, 2006, 24, 1011-1017.	1.9	64

#	Article	IF	CITATIONS
127	Biomechanical and Magnetic Resonance Characteristics of a Cartilage-like Equivalent Generated in a Suspension Culture. Tissue Engineering, 2006, 12, 2755-2764.	4.9	35
128	Biomechanical and Magnetic Resonance Characteristics of a Cartilage-like Equivalent Generated in a Suspension Culture. Tissue Engineering, 2006, .	4.9	0
129	Detection of changes in articular cartilage proteoglycan byT1ï•magnetic resonance imaging. Journal of Orthopaedic Research, 2005, 23, 102-108.	1.2	90
130	Depth-dependent proton magnetization transfer in articular cartilage. Journal of Magnetic Resonance Imaging, 2005, 22, 318-323.	1.9	25
131	Quantification of cartilage biomechanical and biochemical properties viaT1ϕmagnetic resonance imaging. Magnetic Resonance in Medicine, 2005, 54, 1087-1093.	1.9	133
132	T1ϕcontrast in functional magnetic resonance imaging. Magnetic Resonance in Medicine, 2005, 54, 1155-1162.	1.9	29
133	Proteoglycan Loss in Human Knee Cartilage: Quantitation with Sodium MR Imaging—Feasibility Study. Radiology, 2004, 231, 900-905.	3.6	168
134	In vivo measurement of T1? dispersion in the human brain at 1.5 tesla. Journal of Magnetic Resonance Imaging, 2004, 19, 403-409.	1.9	60
135	Correlation of T1? with fixed charge density in cartilage. Journal of Magnetic Resonance Imaging, 2004, 20, 519-525.	1.9	137
136	Pulse sequence for multisliceT1?-weighted MRI. Magnetic Resonance in Medicine, 2004, 51, 362-369.	1.9	31
137	Method for reduced SART1?-weighted MRI. Magnetic Resonance in Medicine, 2004, 51, 1096-1102.	1.9	47
138	Reduction of residual dipolar interaction in cartilage by spin-lock technique. Magnetic Resonance in Medicine, 2004, 52, 1103-1109.	1.9	126
139	In vivo quantification ofT1? using a multislice spin-lock pulse sequence. Magnetic Resonance in Medicine, 2004, 52, 1453-1458.	1.9	51
140	T2?-weighted contrast in MR images of the human brain. Magnetic Resonance in Medicine, 2004, 52, 1223-1227.	1.9	21
141	T1ϕweighted MRI using a surface coil to transmit spin-lock pulses. Journal of Magnetic Resonance, 2004, 167, 306-316.	1.2	12
142	Cartilage volume quantification via Live Wire segmentation1. Academic Radiology, 2004, 11, 1389-1395.	1.3	49
143	Sodium magnetic resonance imaging of proteoglycan depletion in an in vivo model of osteoarthritis1. Academic Radiology, 2004, 11, 21-28.	1.3	72
144	3D-T1ϕrelaxation mapping of articular cartilage. Academic Radiology, 2004, 11, 741-749.	1.3	98

#	Article	IF	CITATIONS
145	Proton MRI of metabolically produced H217O using an efficient 17O2 delivery system. NeuroImage, 2004, 22, 611-618.	2.1	29
146	Proton spin-lock ratio imaging for quantitation of glycosaminoglycans in articular cartilage. Journal of Magnetic Resonance Imaging, 2003, 17, 114-121.	1.9	80
147	Three-dimensional T1?-weighted MRI at 1.5 Tesla. Journal of Magnetic Resonance Imaging, 2003, 17, 730-736.	1.9	59
148	T1?-relaxation mapping of human femoral-tibial cartilage in vivo. Journal of Magnetic Resonance Imaging, 2003, 18, 336-341.	1.9	44
149	Application of the keyhole technique to T1? relaxation mapping. Journal of Magnetic Resonance Imaging, 2003, 18, 745-749.	1.9	29
150	High-resolution assessment of blood flow in murine RIF-1 tumors by monitoring uptake of H217O with protonT1?-weighted imaging. Magnetic Resonance in Medicine, 2003, 49, 1-6.	1.9	27
151	Indirect17O-magnetic resonance imaging of cerebral blood flow in the rat. Magnetic Resonance in Medicine, 2003, 49, 479-487.	1.9	34
152	Artifacts in T1ϕweighted imaging: correction with a self-compensating spin-locking pulse. Journal of Magnetic Resonance, 2003, 162, 113-121.	1.2	99
153	T1ϕMR Imaging of the Human Wrist in Vivo. Academic Radiology, 2003, 10, 614-619.	1.3	27
154	In Vivo Proton MR Three-dimensional T1ϕMapping of Human Articular Cartilage: Initial Experience. Radiology, 2003, 229, 269-274.	3.6	108
155	Quantifying Sodium in the Human Wrist in Vivo by Using MR Imaging. Radiology, 2002, 224, 598-602.	3.6	65
156	Proteoglycan Depletion–Induced Changes in Transverse Relaxation Maps of Cartilage. Academic Radiology, 2002, 9, 1388-1394.	1.3	203
157	Effect of IL-1?-induced macromolecular depletion on residual quadrupolar interaction in articular cartilage. Journal of Magnetic Resonance Imaging, 2002, 15, 315-323.	1.9	14
158	23Na MRI accurately measures fixed charge density in articular cartilage. Magnetic Resonance in Medicine, 2002, 47, 284-291.	1.9	263
159	Fast MRI of RF heating via phase difference mapping. Magnetic Resonance in Medicine, 2002, 47, 492-498.	1.9	24
160	T1ϕImaging of Murine Brain Tumors at 4 T. Academic Radiology, 2001, 8, 42-47.	1.3	44
161	Proteoglycan-induced changes inT1?-relaxation of articular cartilage at 4T. Magnetic Resonance in Medicine, 2001, 46, 419-423.	1.9	351
162	Preferential incorporation of glucosamine into the galactosamine moieties of chondroitin sulfates in articular cartilage explants. Arthritis and Rheumatism, 2001, 44, 1089-1095.	6.7	51

#	Article	IF	CITATIONS
163	Human Knee: In Vivo T1ϕweighted MR Imaging at 1.5 T—Preliminary Experience. Radiology, 2001, 220, 822-826.	3.6	124
164	Demonstration of a compact compressor for application of metastability-exchange optical pumping of3He to human lung imaging. Magnetic Resonance in Medicine, 2000, 43, 290-294.	1.9	29
165	Sodium Visibility and Quantitation in Intact Bovine Articular Cartilage Using High Field 23Na MRI and MRS. Journal of Magnetic Resonance, 2000, 142, 24-31.	1.2	113
166	Time-Domain Quantification of Multiple-Quantum-Filtered 23Na Signal Using Continuous Wavelet Transform Analysis. Journal of Magnetic Resonance, 2000, 142, 341-347.	1.2	8
167	17O-Decoupled 1H Spectroscopy and Imaging with a Surface Coil: STEAM Decoupling. Journal of Magnetic Resonance, 2000, 143, 39-44.	1.2	11
168	Temperature-Dependent Chemical Shift and Relaxation Times of 23Na in Na4HTm[DOTP]. Journal of Magnetic Resonance, 2000, 143, 213-216.	1.2	10
169	Intermolecular Dipole–Dipole Relaxation of 129Xe Dissolved in Water. Journal of Magnetic Resonance, 2000, 145, 302-306.	1.2	10
170	MR imaging of RF heating using a paramagnetic doped agarose phantom. Magnetic Resonance Materials in Physics, Biology, and Medicine, 2000, 10, 114-121.	1.1	18
171	Demonstration of a compact compressor for application of metastability-exchange optical pumping of 3He to human lung imaging. , 2000, 43, 290.		2
172	An MR imaging method for simultaneous measurement of gaseous diffusion constant and longitudinal relaxation time. Magnetic Resonance Imaging, 1999, 17, 267-273.	1.0	11
173	Contributory presentations/posters. Journal of Biosciences, 1999, 24, 33-198.	0.5	Ο
174	In Vivo Triple Quantum Filtered Twisted Projection Sodium MRI of Human Articular Cartilage. Journal of Magnetic Resonance, 1999, 141, 286-290.	1.2	78
175	Detection of residual quadrupolar interaction in the human breast in vivo using sodium-23 multiple quantum spectroscopy. Journal of Magnetic Resonance Imaging, 1999, 9, 391-394.	1.9	9
176	A novel approach to observing articular cartilage deformation in vitro via magnetic resonance imaging. Journal of Magnetic Resonance Imaging, 1999, 9, 653-662.	1.9	44
177	Sodium and proton MR properties of cartilage during compression. Journal of Magnetic Resonance Imaging, 1999, 10, 961-967.	1.9	48
178	Sodium NMR evaluation of articular cartilage degradation. Magnetic Resonance in Medicine, 1999, 41, 30-34.	1.9	82
179	Off-resonance proton T1p dispersion imaging of170-enriched tissue phantoms. Magnetic Resonance in Medicine, 1998, 39, 588-595.	1.9	23
180	Sodium MRI of human articular cartilagein vivo. Magnetic Resonance in Medicine, 1998, 39, 697-701.	1.9	218

#	Article	IF	CITATIONS
181	MRI of hyperpolarized3He gas in human paranasal sinuses. Magnetic Resonance in Medicine, 1998, 39, 865-868.	1.9	19
182	Sodium multiple quantum spectroscopy of articular cartilage: Effects of mechanical compression. Magnetic Resonance in Medicine, 1998, 40, 370-375.	1.9	11
183	Proton T1ϕdispersion imaging of rodent brain at 1.9 T. Journal of Magnetic Resonance Imaging, 1998, 8, 1090-1096.	1.9	25
184	High resolution, short echo time sodium imaging of articular cartilage. Journal of Magnetic Resonance Imaging, 1997, 7, 1056-1059.	1.9	32
185	In Vivo sodium multiple quantum spectroscopy of human articular cartilage. Magnetic Resonance in Medicine, 1997, 38, 207-214.	1.9	52
186	Triple quantum sodium imaging of articular cartilage. Magnetic Resonance in Medicine, 1997, 38, 279-284.	1.9	27
187	A simplified sequence for observing deoxymyoglobin signalsin vivo: Myoglobin excitation with dynamic unexcitation and saturation of water and fat (MEDUSA). Magnetic Resonance in Medicine, 1997, 38, 788-792.	1.9	13
188	T1ϕrelaxation in articular cartilage: Effects of enzymatic degradation. Magnetic Resonance in Medicine, 1997, 38, 863-867.	1.9	300
189	17O-Decoupled Proton MR Spectroscopy and Imaging in a Tissue Model. Journal of Magnetic Resonance, 1997, 125, 1-7.	1.2	26
190	17O-decoupled 1H detection using a double-tuned coil. Magnetic Resonance Imaging, 1996, 14, 1073-1078.	1.0	26
191	Detection of Residual Quadrupolar Interaction in Human Skeletal Muscle and Brain in vivo via Multiple Quantum Filtered Sodium NMR Spectra. Magnetic Resonance in Medicine, 1995, 33, 134-139.	1.9	60
192	Spectral localization of arbitrarily shaped regions of interest (SLASH) using single voxel signals. Magnetic Resonance Imaging, 1993, 11, 1203-1208.	1.0	1
193	Sensitivity ofin vivo mrs of the n-î´ proton in proximal histidine of deoxymyoglobin. Magnetic Resonance in Medicine, 1992, 27, 362-367.	1.9	23
194	Longitudinal spin-order-based pulse sequence for lactate editing. Magnetic Resonance in Medicine, 1991, 19, 477-482.	1.9	17
195	Application of tensor operator formalism in pulsed nuclear quadrupole resonance spectroscopy. Molecular Physics, 1991, 72, 491-507.	0.8	14
196	Application of tensor operator formalism in pulsed nuclear quadrupole resonance spectroscopy. Molecular Physics, 1991, 72, 509-521.	0.8	9
197	Double quantum coherence in pure nuclear quadrupole resonance spectroscopy. Journal of Molecular Structure, 1989, 192, 309-319.	1.8	5